Journal of Ceramic Processing Research. Vol. 10, No. 5, pp. 669~673 (2009)

J O U R N A L O F
Ceramic Processing Research

Formation of hydroxyapatite nanoneedles on the surface of a novel calcium phosphate/blood plasma proteins biocement in simulated body fluid (SBF)

Mahdi Rezvannia, Fathollah Moztarzadeh and Mohammadreza Tahriri *

Biomaterials Group, Faculty of Biomedical Engineering (Center of Excellence), Amirkabir University of Technology, P.O. Box: 15875-4413, Tehran, Iran

In this study, we report on needle-like hydroxyapatite grown on the surface of calcium phosphate/blood plasma proteins biocement in simulated body fluid (SBF). Scanning electron microscope revealed the formation of nano-sized needle-like hydroxyapatite crystals on the surface of the biocement after 7 days immersion in the simulated body fluid. X-ray diffraction analysis of the biocement structures indicated that the nanoneedle crystals were hydroxyapatite. Finally Fourier transform infra-red investigations were employed to detect the functional groups of the biocement which this technique demonstrated to be hydroxyapatite.

Key words: Biocement, Nanoneedles, Hydroxyapatite, Calcium phosphate.

Introduction

Several calcium phosphate cements (CPC) have been developed since the proposal of using apatitic calcium phosphates as restorative materials in 1982 and the first self-setting calcium phosphate cement reported in 1986 [1, 2].

Calcium phosphate cements generally consist of a powder and an aqueous liquid, which are mixed to form a paste [2-8]. The paste is placed into a defect as a substitute for the damaged part of bone [9-14]. One calcium phosphate cement, referred to as CPC [2, 12, 13], consists of tetracalcium phosphate (TTCP, $Ca_4(PO_4)O$) and dicalcium phosphate anhydrous (DCPA, $CaHPO_4$). The CPC paste intimately adapts to the bone cavity even for irregularly shaped cavities. CPC forms hydroxyapatite in an aqueous environment at body temperature, hence it is more similar to biological apatites than sintered hydroxyapatite formed at high temperatures [15]. As a result, CPC is not only bioactive, noncytotoxic and osteoconductive, it is also bioresorbable and can be replaced by new bone [9-13].

In recent years significant research effort has been devoted to developing inorganic nanocrystals because of their potential applications in biology, electronics, optics, transport and information technology. Although several approaches have investigated ways of making these nanocrystals, controlling the size, shape and crystalinity and various parameters affecting the size and shape of these materials still need to be found [16].

*Corresponding author:
Tel : +98-21-44218562
Fax: +98-21-66468186
E-mail: m-tahriri@aut.ac.ir

Nanosized hydroxyapatite (HA) is the main component of mineral bone. Living bone constantly undergoes a coupled resorptive-formative process known as bone remodeling. The process involves simultaneous bone removal and replacement through the respective activities of osteoblasts and osteoclasts, with the accompanying vascular supply and a network of canaliculi and lacunae [17]. HA possesses exceptional biocompatibility and bioactivity properties with respect to bone cells and tissues, probably due to its similarity with the hard tissues of the body [18-23]. Calcium phosphate materials form the main mineral part of calcified tissues. However, the presence of calcium phosphate in bone is in the form of nanometre-sized needle-like crystals of approximately 5-20 nm width by 60 nm length, with a poorly crystallized non-stoichiometric apatite phase containing CO_3^{2-}, Na^+, F^- and other ions in a collagen fiber matrix. Current research deals with new HA formulations aiming at better and more effective biomedical applications, producing this material with properties closer to those of living bone, such as nanosized and monolithic structures [17].

It is believed that nanostructured calcium phosphate ceramics for example, nanosize needle-like hydroxyapatite can improve the sintering kinetics due to a higher surface area and subsequently improve mechanical properties significantly [24].

In this investigation, we are reporting creation of hydroxyapatite nanoneedles on the surface of the fabricated cement from a mixture of tetracalcium phosphate/ anhydrous dicalcium phosphate as the solid phase and blood plasma proteins as liquid phase. The reason for using blood plasma proteins as a liquid phase in this research was enhancement of cement biocompatibility.

Experimental

Biocement powder

The starting materials used as cement in the present study are, tetracalcium phosphate (TTCP; $Ca_4(PO_4)O$) and anhydrous dicalcium phosphate (DCPA; $CaHPO_4$).

At first, tetracalcium phosphate was synthesized by the solid-state reaction of an equimolar mixture of calcium carbonate and anhydrous dicalcium phosphate (Ca/P molar ratio = 2.0) at 1500 °C for 6 hours. The tetracalcium phosphate was powdered in a satellite miller for 25 minutes. Also, anhydrous dicalcium phosphate (DCPA) was acquired from the Merck Company Inc. (No. 2144). Then, the particle size distribution of the milled TTCP and prepared DCPA was determined by a laser particle size analyzer (LSPA; Fritsch particle size analyser 22). Fig. 1 shows particle size distribution curves of milled TTCP and prepared DCPA.

According to these curves, the mean particle size of TTCP was determined to be about 9.57 μm. So that 95% of the particles had a size less than 21.74 μm and 75% of the particles had a size less than 14 μm. Also the mean particle size of DCPA was determined to be about 7.64 μm. So that 95% of the particles had a size less than 17.5 μm and 75% of the particles had a size less than 11 μm. Therefore, the mean particle size of DCPA was a little less than the mean particle size of TTCP.

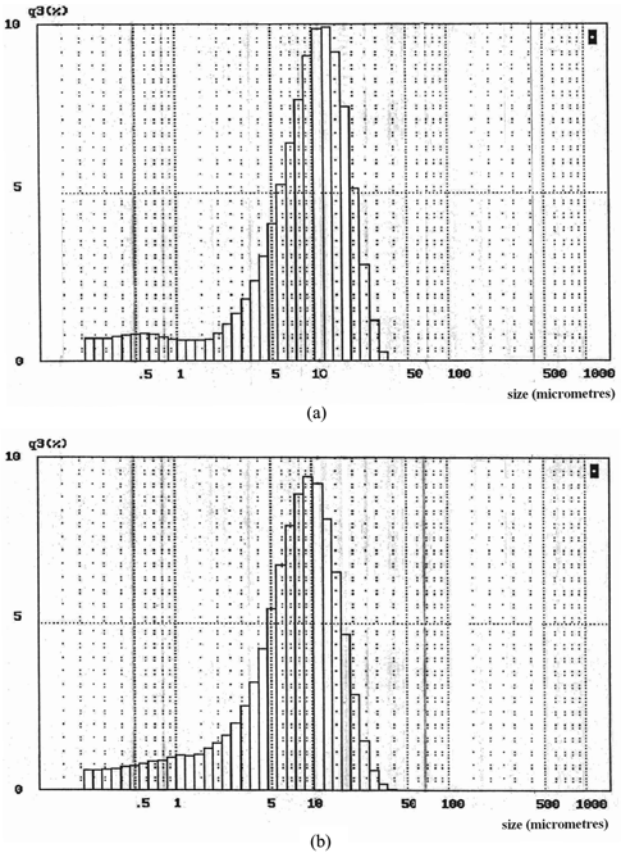

Fig. 1. Particle size distribution curves of (a) milled TTCP and (b) prepared DCPA.

TTCP and DCPA powders were mixed at a molar ratio of 1 : 1 to form the cement powder.

Biocement liquid

The biocement liquid used in this study was human blood plasma. The reason for using blood plasma as a liquid phase in this study was an improvement of the biocompatibility of the biocement. The elemental composition of the human blood plasma is shown in Table 1.

Biocement sample preparation

The flowchart for the preparation of the biocement is illustrated in Fig. 2.

At first, human blood plasma was centrifuged for 15 minutes at a rate of 2000 rpm until the proteins of the blood plasma were separated. In the next step, the biocement sample which consisted of 0.5 ml blood plasma proteins and 2 g TTCP/DCPA with a 1 : 1 molar ratio was prepared. This biocement was dried in air for 24 hours and the whole thing was soaked in 30 ml simulated body fluid solution (SBF) for 7 days and it was then washed with de-ionized water and lastly, placed in air for 24 hours. The SBF solution was prepared by

Table 1. Inorganic part of human blood plasma (mmol/l)

Ion	Plasma (*mmol/l*)
Na^+	142.0
K^+	5.0
Mg^{+2}	1.5
Ca^{+2}	2.5
Cl^-	103.0
HCO_3^-	27
HPO_4^{-2}	1.0
SO_4^{-2}	0.5

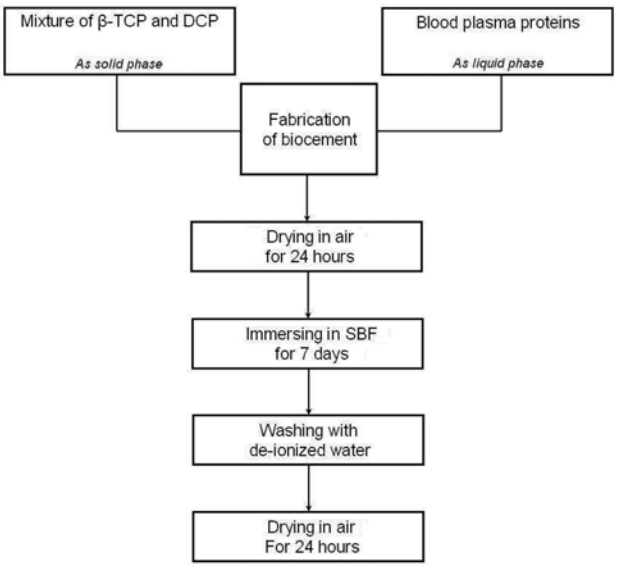

Fig. 2. Flowchart for processes of the formation of the hydroxyapatite nanoneedles.

Table 2. Composition of SBF(mmol/l)

Ion	SBF (*mmol/l*)
Na^{+}	142.0
K^{+}	5.0
Mg^{+2}	1.5
Ca^{+2}	2.5
Cl^{-}	147.8
HCO_3^{-}	4.2
HPO_4^{-2}	1.0
SO_4^{-2}	0.5

dissolving reagent-grade NaCl, KCl, $NaHCO_3$, $MgCl_2 .6H_2O$, $CaCl_2$ and KH_2PO_4 into distilled water and buffered at pH = 7.25 with TRIS (trishydroxymethyl aminomethane) and 1N HCl at 37 °C. Its composition is given in Table 2.

Biocement characterization

X-ray diffraction

The resulting powder was analyzed by X-ray diffraction (XRD) with a Philips PW 3710. This instrument was used with voltage and current settings of 30 kV and 25 mA respectively and used Cu-Kα radiation (1.540510 Å). For qualitative analysis, XRD diagrams were recorded in the interval $10^{o} \leq 2\theta \leq 80^{o}$ at a scan speed of 2°/minute.

Fourier transform infra-red

The powder sample was examined by Fourier transform infra-red with a Bomem MB 100 spectrometer. For IR analysis, at first 1 mg of the powder sample was carefully mixed with 300 mg of KBr (infrared grade) and palletized under a vacuum. Then the pellet was analyzed in the range of 400 to 4000 cm^{-1} at a scan speed of 23 scan/min with a 4 cm^{-1} resolution.

Scanning electron microscope

The biocement sample was sputter coated with a thin layer of gold (EMITECH K450X, England) and then the microstructure of the biocement sample was observed in a scanning electron microscope (SEM; Tescan Vega 2XMU) that was operated at an acceleration voltage of 15 kV.

Result and discussion

XRD analysis

The biocement specimen was analyzed by XRD to determine the formation of hydroxyapatite crystals in the specimen. Fig. 3 shows the XRD pattern of the biocement.

As shown in Fig. 3, the biocement has a low degree of crystallinity. It can also be seen in this figure, that the peaks corresponding to hydroxyapatite are clearly identified. Therefore the nano-sized needle-like crystals formed in the biocement are hydroxyapatite.

FT-IR analysis

An FTIR investigation was employed for the detection

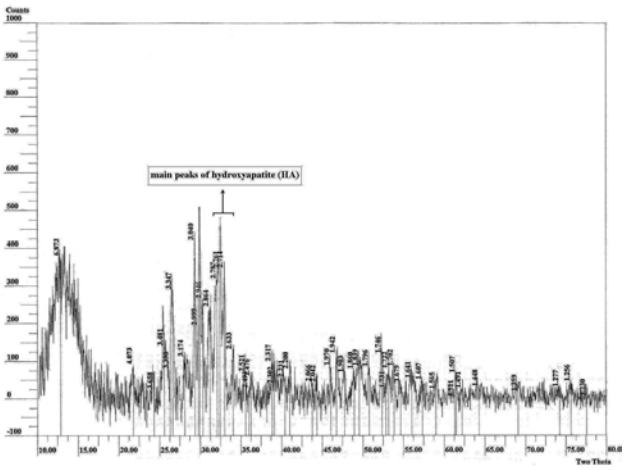

Fig. 3. XRD pattern of the cement produced.

of functional group bonds of the biocement fabricated. Fig. 4 shows the FTIR spectra of the biocement powder.

The characteristic bands (listed in Table 3) exhibited in the sample spectra assigned here (a) two bands were observed at 3401.92 cm^{-1} and 620.019 cm^{-1} due to the stretching mode of hydrogen-bonded OH^{-} ions and vibrational mode of hydrogen-bonded OH^{-} ions respectively. (b) The band at 1063.72 cm^{-1} arises from ν_3 PO_4, the bands at 602.44 cm^{-1} and 567.916 cm^{-1} arise from ν_4 PO_4, the bands at 504.439 cm^{-1} and 471.393 cm^{-1} arise from ν_2 PO_4 [25, 26]. (c) The bands at 1417.35 cm^{-1} and 1641.11 cm^{-1} arise from CO_3 ions. Therefore the FTIR analysis showed all the typical absorption characteristics of hydroxyapatite. In addition, some carbonate content also was seen, which is an indication of the presence of

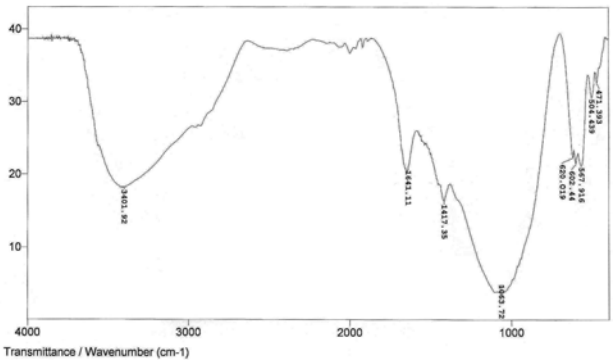

Fig. 4. FTIR spectra of the cement powder produced.

Table 3. Infrared bands aassigned for the cement fabricated

Assignment	Infrared frequency (cm^{-1})
OH^{-} stretching	3401.02
CO_3^{-2}	1641.11, 1417.35
ν_3 PO_4^{-3} stretch	1063.72
OH^{-} vibrational	620.019
ν_4 PO_4^{-3} bend	602.44 , 567.916
ν_2 PO_4^{-3} bend	504.439 , 471.393

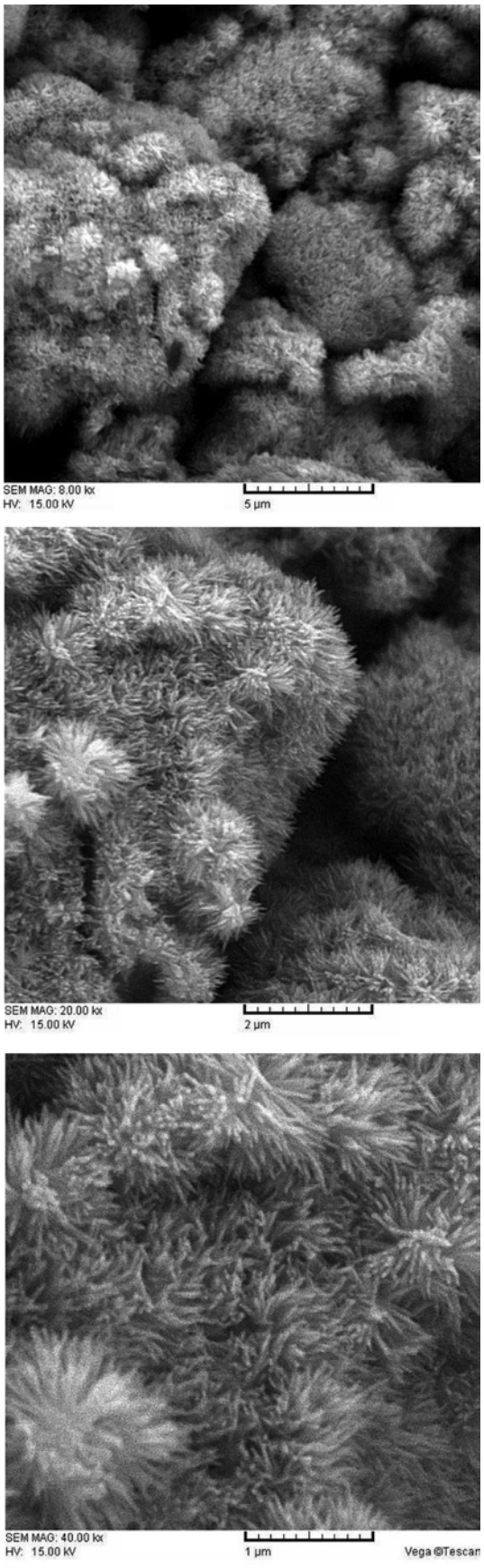

Fig. 5. SEM micrographs of the cement surface and observation of hydroxyapatite nanoneedles at different magnifications.

carbonate apatite. This might have originated through the absorption of carbon dioxide from the atmosphere [25].

SEM observations

A SEM was used to examine the biocement specimen and to observe the morphology of the biocement, especially needle-like hydroxyapatite crystals and to estimate the length and diameter of nanoneedle crystals. SEM micrographs of biocement at different magnifications are shown in Fig. 5.

SEM revealed the formation of nano-sized needle-like hydroxyapatite crystals on the surface of the biocement after 7 days immersion in the simulated body fluid (SBF). This technique showed that nanoneedles were straight with sharp tips. This can also be seen in this figure, where some of the nanoneedles crossed each other.

Conclusions

In conclusion, we reported the creation of nanosized needle-like hydroxyapatite crystals on a new calcium phosphate/blood plasma proteins cement.

The XRD analysis showed that nanosize needle-like crystals formed on the surface of the cement were hydroxyapatite. The FTIR investigation also showed all the typical absorption characteristics of hydroxyapatite. The SEM technique revealed the creation of nanosized needle-liked hydroxyapatite crystals on the surface of the cement after 7 days soaking in the simulated body fluid (SBF). This technique also showed that all of the needles had nanometre-sized diameter and sub-micrometre lengths.

Finally, the newly produced cement in this study had not been reported before, and this novel cement also had the ability to create hydroxyapatite nanoneedles on its surface.

Acknowledgements

The authors would like to acknowledge Dr. S. Kordestani for helping with this investigation.

References

1. R.Z. LeGeros, A. Chohayeb, A. Shulman, J. Dent. Res. 61 (1982) 343-347.
2. L.E. Carey, H.H.K. Xu and C.G. Simon, Biomaterials 26 (2005) 5002-5014.
3. M.P. Ginebra, E. Fernandez, E.A.P. De Maeyer, Verbeeck, R.M.H. M.G Boltong, J. Ginebra, F.C.M. Driessens and J.A. Planell, J. Dent. Res. 76 (1997) 905-912.
4. B.R. Constantz, B.M. Barr, I.C. Ison, M.T. Fulmer, J. Baker, L. McKinney, S.B. Goodman, S. Gunasekaren, D.C. Delaney, J. Ross, R.D. Poser and J. Biomed. Mater. Res. (Appl. Biomater.) 43 (1998) 451-461.
5. D. Knaack, M.E.P. Goad, M. Aiolova, C. Rey, A. Tofighi, P. Chakravarthy, D.D. Lee and J. Biomed. Mater. Res. (Appl. Biomater.) 43 (1998) 399-409.
6. Y. Miyamoto, K. Ishikawa, M. Takechi, T. Toh, T. Yuasa, M. Nagayama, K. Suzuki and J. Biomed. Mater. Res. (Appl. Biomater.) 48 (1999) 36-42.

7. J.E. Barralet, T. Gaunt, A.J. Wright, I.R. Gibson, J.C. Knowles and J. Biomed. Mater. Res (Appl. Biomater.) 63 (2002) 1-9.
8. A. Yokoyama, S. Yamamoto, T. Kawasaki, T. Kohgo and M. Nakasu, Biomaterials 23 (2002) 1091-1101.
9. C.D. Friedman, P.D. Costantino, K. Jones, L.C. Chow, H.J. Pelzer and G.A. Sisson, Arch. Otolaryngol. Head Neck Surg. 117 (1991) 385-389.
10. P.D. Costantino, C.D. Friedman, K. Jones, L.C. Chow and G. A. Sisson, Plast. Reconstr. Surg. 90 (1992) 174-191.
11. M.L. Shindo, P.D. Contantino, C.D. Friedman and L.C. Chow: Arch. Otolaryngol. Head Neck Surg. 119 (1993) 185-190.
12. C.D. Friedman, P.D. Costantino, S. Takagi, L.C. Chow and J. Biomed. Mater. Res. (Appl. Biomater.) 43 (1998) 428-432.
13. L.C. Chow, Mater. Res Symp. Proc. 599 (2000) 27-37.
14. D. Apelt, F. Theiss, A.O. El-Warrak, K. Zlinszky, R. Bettschart-Wolfisberger, M. Bohner, S. Matter and J.A. Auer, B. von Rechenberg, Biomaterials 25 (2004) 1439-1451.
15. S. Takagi, L.C. Chow, M. Markovic, C.D. Friedman, P.D. Costantino and J. Biomed. Mater. Res. (Appl. Biomater.) 58 (2001) 36-41.
16. H. Eslami, M. Solati-Hashjin and M. Tahriri, J. Ceram. Process. Res. 9 (2008) 224-229.
17. M.P. Ferraz, F.J. Monteiro and C.M. Manuel, J. Appl. Biomaterials & Biomechanics 2 (2004) 74-80.
18. T. Kokubo, H. M. Kim and M. Kawashita, Biomaterials 24 (2003) 2161-2175.
19. M. Kikuchi, S. Itoh, S. Ichinose, K. Shinomiya and J. Tanaka, Biomaterials 22 (2001) 1705-1711.
20. R. Schnettler, V. Alt, E. Dingeldein, H.J. Pfefferle, O. Kilian, C. Meyer, C. Heiss and S. Wenisch, Biomaterials 24 (2003) 4603-4608.
21. S. C. Liou, S. Y. Chen and D. M. Liu, Biomaterials 24 (2003) 3981-3988.
22. U. Vijayalakshmi and S. Rajeswari, Trends Biomater. Artif. Organs 19(2) 2006 57-62.
23. M. H. Santos, M.D. Oliveira, L.P.D. F. Souza, H.S. Mansur and W.L. Vasconcelos, Mat. Res. 7 (2004), 625-630.
24. S. Bose and S.K. Saha, J. Am. Ceram. Soc. 86 (2003) 1055-1057.
25. N. Rameshbabu, T.S. Sampath Kumar and K. Prasad Rao, Bull. Mater. Sci. 29 (2006) 611-615.
26. M. Komath and H.K. Varma, Bull. Mater. Sci. 4 (2003) 415-422.